journal

J. Am. Ceram. Soc., **95** [4] 1414–1420 (2012)
DOI: 10.1111/j.1551-2916.2012.05076.x

Heterostructured Ceramic Powders for Photocatalytic Hydrogen Production: Nanostructured TiO_2 Shells Surrounding Microcrystalline (Ba,Sr)TiO_3 Cores

Li Li, Gregory S. Rohrer, and Paul A. Salvador†

Department of Materials Science and Engineering, Carnegie Mellon University, Pittsburgh, Pennsylvania 15213

Heterostructured photocatalysts were prepared to have nanostructured (*ns*) TiO_2 shells surrounding microcrystalline (*mc*) cores of (Ba,Sr)TiO_3. The as-prepared heterostructures were annealed between 400°C and 600°C to improve crystallinity and core-shell interfacial bonding. X-ray diffraction, electron microscopy, and gas adsorption measurements demonstrated that 50 nm thick shells composed of nanocrystalline and nanoporous TiO_2 surrounded *mc*-cores such that the heterostructured particles had surface areas of 50–100 m^2/g. The *mc*-(Ba,Sr)TiO_3/*ns*-TiO_2 core-shell photocatalysts annealed at 600°C had slightly reduced surface areas, but had the highest rates of photochemical hydrogen production from water/methanol solutions, rates much greater than those for *ns*-TiO_2 or *mc*-(Ba,Sr)TiO_3 alone. Such heterostructured powders represent a new strategy for the design of efficient photocatalysts and the use of nanostructured catalytic coatings.

I. Introduction

Interest in photochemical hydrogen production began several decades ago upon the discovery that TiO_2 could catalyze the photo-induced (UV) dissociation of water (photolysis).[1] The fundamental science governing photolysis using ceramic catalysts is now well established and photolytic hydrogen production using powder catalysts offers an inexpensive scalable method for solar energy conversion.[1–6] While over 130 materials are known to split water photochemically, the conversion efficiency of light energy to hydrogen is unacceptably low for all of them.[5] The physicochemical properties required to catalyze photolysis efficiently and sustainably are very restrictive; it is difficult to optimize them individually within a single material.[5,7] Heterostructured photocatalysts offer extra degrees of freedom in material design to improve the efficiency of photolysis.[8] Mixtures of materials[9–11] and core-shell nanocatalysts[12–17] have both been investigated to optimize specific processes, such as light absorption, or structural features, such as surface areas.

Two important processes limit the efficiency of photocatalysts: recombination of photogenerated charge carriers and back reaction of intermediate chemical species.[18] An ideal photocatalyst absorbs all light in a space charge region, allowing efficient separation of the photogenerated carriers. For a semiconducting photocatalyst with a sufficiently large crystal size, space charge regions are ≈0.1–1 μm wide, with absorption depths being similar for photons of interest. The surface area of such particles is too low for efficient catalysis. High surface area nanostructured powders are better for catalysis, but they do not support internal space charges,[19] and only separate photogenerated carriers if the electronic energy levels in each component are optimized.[9,10] Moreover, intermediate reactions are not separated spatially for surfaces with local heterogeneities or for nanoparticles, and back reactions are problematic.[2,6,18] Photoelectrochemical systems use an internal voltage to separate the photogenerated carriers, and therefore the chemical reactions, over macroscopic distances.[2–4] The ultimate aim in photolysis is to achieve particle equivalents of photoelectrochemical cells.[3,20] Here we demonstrate that heterostructured ceramic powders can be prepared in which the length scales for light absorption, charge separation and transfer, and photochemical reaction can be independently controlled.

Internal electric fields can also be used to separate photogenerated carriers and to control the spatial location of photochemical processes. In powder photocatalysts, internal fields arise from mismatches in the electrochemical potential of electrons at interfaces.[2,7,18,21] When light is absorbed in an electric field, the electron and hole move in opposite directions. Of course, it is of interest to control the field specifically at the surface of the particle to ensure different spatial locations support oxidation and reduction. This is often done through the impregnation of nanoscale metallic co-catalysts.[5,6] Polar surface terminations can also influence the internal field in the catalyst.[22] Similarly, the internal dipolar field in ferroelectrics modifies the native surface fields to promote either photochemical oxidation or reduction, depending on the orientation of the polarization at the surface.[21,23–33] We present here examples of hierarchically structured photocatalysts that allow for light absorption to occur in space charge regions, and that transfer photogenerated carriers to high surface area catalytic shells.

TiO_2 still attracts the most interest of all photocatalysts because it has a workable balance of the necessary material properties for photocatalysis.[5,6,34,35] Recently, we showed that the surface reactivity of thin (<100 nm) dense TiO_2 coatings supported on ferroelectrics ($BaTiO_3$) was directly influenced by the underlying ferroelectric domain structure.[21] Moreover, carriers photogenerated in the ferroelectric participated in the reactivity of the TiO_2 film,[29,30] akin to a light absorbing core—reactive shell nanocatalyst. Moreover, the phase and orientation reactivity differences of bulk TiO_2 were overshadowed entirely by the ferroelectric substrate.[29,30] These results suggest that heterostructured photocatalysts could be designed in which the absorption/charge separation properties of a core having internal fields could be combined with a nanostructured shell of high surface area and favorable band edge locations to improve the efficiency of water splitting. Along these lines, it was demonstrated that nanostructured TiO_2 coatings on microcrystalline $FeTiO_3$ had improved properties for the degradation of organic dyes[16] and that CdS–TiO_2 nano-bulk composites exhibit improved hydrogen production under visible light.[36,37] In those heterostructures, the primary role of the bulk is to absorb visible light. Here, we fabricate and characterize heterostructured photocatalysts composed of microcrystalline (*mc*) cores of (Ba,Sr)TiO_3 and nanostructured (*ns*) shells of TiO_2, and test if they lead to hydrogen generation from water, yielding a

E. Dickey—contributing editor

Manuscript No. 30282. Received September 06, 2011; approved December 21, 2011.
†Author to whom correspondence should be addressed. e-mail : paulsalvador@cmu.edu

new strategy for the photocatalyst design in which the physical length scales of the heterostructured powders can be well matched to light absorption and charge separation.

II. Experimental Procedure

Micron-sized powders of $BaTiO_3$ (99.7%; Alpha Aesar, Ward Hill, MA) and $SrTiO_3$ (>99%; Acros Organics, Morristown, NJ) were used as precursors to prepare faceted microcrystals. Faceted $BaTiO_3$ and $SrTiO_3$ powders were synthesized by a molten salt flux method.[28] Equal weights of $BaTiO_3$ and KCl (>99%; Acros Organics) were combined with ethanol, ball milled for several minutes, stirred continuously for 2 h, and dried at 70°C for 12 h. The dried powder was transferred to an Al_2O_3 crucible and calcined at 1100°C for 5 h with 5°C/min heating/cooling rates. KCl was removed by filtering with boiling water and washing repeatedly with distilled water. The faceted powder was dried at 70°C for 12 h.

Nanostructured (*ns*-)TiO_2 was prepared by the hydrolysis of titanium (IV) *n*-butoxide[17,38] (TBOT; 99.0%, Acros Organics), either as a free-standing powder or coated on microcrystalline (*mc*-) $BaTiO_3$, $SrTiO_3$, and Al_2O_3. A mixture of 9 mL water and 20 mL ethanol was prepared. When used, core powders (≈1 g) were added to the mixture and ultrasonically dispersed for 0.5 h. HCl was added to the water/ethanol solutions to adjust the pH to ≈3–4 (except with Al_2O_3 cores, where pH was ≈5–6). Another solution was prepared with a suitable amount (15 mL) of ethanol, 8.6 mL TBOT, and 1 mL of 2,4-pentanedione. The TBOT solution was added drop-wise to the water/ethanol solution over ≈15 min. The mixture was stirred vigorously for 2 h and then aged at 90°C in a water bath for 9 h while stirring at 300 rpm. The as-prepared product was obtained by centrifugation of the aged mixture, washing several times with ethanol, and drying at 80°C for 24 h. Several control samples were also obtained. Mechanical mixtures of similar compositions to the heterostructured powders were prepared by: mixing core powders with Degussa P25 (Degussa, Parsippany, NJ) in ethanol, treating them sonomechanically for 3 h using an ultrasonic bath at 80°C, and drying them at 70°C for 12 h. The same sonomechanical procedure was used to treat Degussa P25. Some of the as-prepared powders were sintered in air for 2 h at temperatures between 400°C and 600°C; they were heated and cooled at 5°C/min.

θ-2θ X-ray diffraction patterns were registered using a diffractometer (PANalytical; X'Pert Pro, Philips, Almelo, the Netherlands) equipped with Cu$K\alpha$ radiation, operated at 45 kV and 40 mA, and scanned at 3°/min with data collected at a step size of 0.05°. For transmission electron microscopy (2000EX; JEOL, Peabody, MA), powders were ultrasonically dispersed in methanol and several drops of the suspension were placed on a 200 mesh copper grid coated with a carbon support film. Nitrogen adsorption-desorption measurements (Nova 2200e; Quantachrome, Boynton Beach, FL) were carried out at 77 K, using a multipoint method, after vacuum-degassing for 3 h at 300°C. Surface area and pore size distributions were determined using the Brunauer–Emmett–Teller (BET) and the Barret–Joyner–Halenda (BJH) model, respectively. The pore volume was measured at the $P/P_0 = 0.99$ point.

All powders tested photocatalytically were loaded with 1 wt% Pt by an impregnation-reduction method.[39,40] Determined quantities of powders and H_2PtCl_6 solution were mixed and stirred for 2 h. A fivefold excess of a NaOH and $NaBH_4$ solution was added and stirred for 2 h. The powders were collected by centrifugation, rinsed with distilled water, and dried at 70°C for 12 h. A gas-tight reactor system (similar to those described elsewhere)[41] equipped with a 450 W medium-pressure mercury immersion lamp (ACE Glass, Vineland, NJ) was used for measuring hydrogen generation. The lamp was inserted into a borosilicate immersion well (ACE Glass), held inside a 500 mL inner reaction chamber, that transmitted wavelengths >280 nm. The reaction vessel was maintained at room temperature with flowing water. A certain mass (0.4 g or ~1 wt%) of photocatalyst was added to a distilled water/methanol (92/8 mL) solution and placed in the outer reaction chamber. Methanol is a common sacrificial reagent that scavenges holes, forming CO_2 rather than O_2.[6,42,43] The system was evacuated several times and the pressure prior to reaction was 5 torr. The volume of hydrogen produced was quantified by periodically withdrawing gas from the headspace in the reactor using a 0.5 mL syringe and injecting it into a gas chromatograph (Shimadzu, Columbia, MD; GC-14A, TCD, Ar carrier). Experiments conducted in the dark, or with no photocatalyst, under otherwise identical conditions yielded no detectable hydrogen for all catalysts.

III. Results and Discussion

(1) Phase and Heterostructure Characterization

The XRD patterns of representative photocatalysts are given in Fig. 1. All peaks could be indexed to $BaTiO_3$ (JCPDS 05-0626), anatase (A) TiO_2 (JCPDS 46-1237), or rutile (R) TiO_2 (JCPDS 33-1381). The *ns*-TiO_2 (annealed at 500°C) and P25 have similar patterns, with slight differences in the peak widths and the relative ratio of anatase to rutile. Although these effects are slight, the photocatalytic properties of TiO_2 are affected by crystalline quality and phase composition.[44,45] No evidence of reaction was observed for the $TiO_2/BaTiO_3$ systems. Similar results were observed for the other systems described herein.

In Fig. 2, bright field (BF) TEM images are shown for the Pt-impregnated *mc*-$BaTiO_3$ core/*ns*-TiO_2 shell powders annealed at 600°C and 400°C [their XRD patterns were similar to Fig. 1(d)]. The dark region corresponds to the micron-sized $BaTiO_3$ crystallite, the light gray regions to free space, and the interfacial region with mottled contrast to the *ns*-TiO_2 shell. The interface between the core and shell is sharp and clear in Fig. 2(a), at low magnification; at higher magnification, the interface is less clear because of particle curvature and variations in the coating thickness. The *ns*-TiO_2 shell surrounds the $BaTiO_3$ microcrystal, although the local thickness varies. Higher magnification images, one is given in Fig. 2(b), show details of the coating nanostructure and mor-

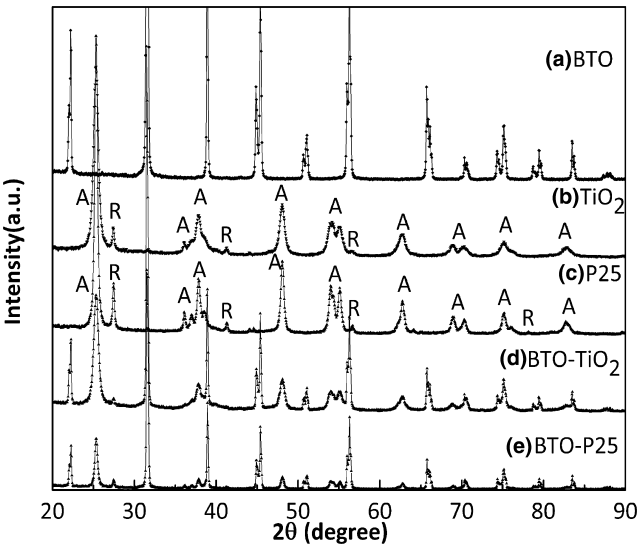

Fig. 1. Powder X-ray diffractograms of (a) *mc*-$BaTiO_3$ (BTO), (b) *ns*-TiO_2 annealed at 500°C, (c) Degussa P25, (d) heterostructured *mc*-$BaTiO_3$ core/*ns*-TiO_2 shell annealed at 500°C, and (e) a sonomechanical mixture of *mc*-$BaTiO_3$ and P25. All peaks in (a) correspond to those of $BaTiO_3$. In (b) and (c), peaks associated with anatase (A) and rutile (R) are marked.

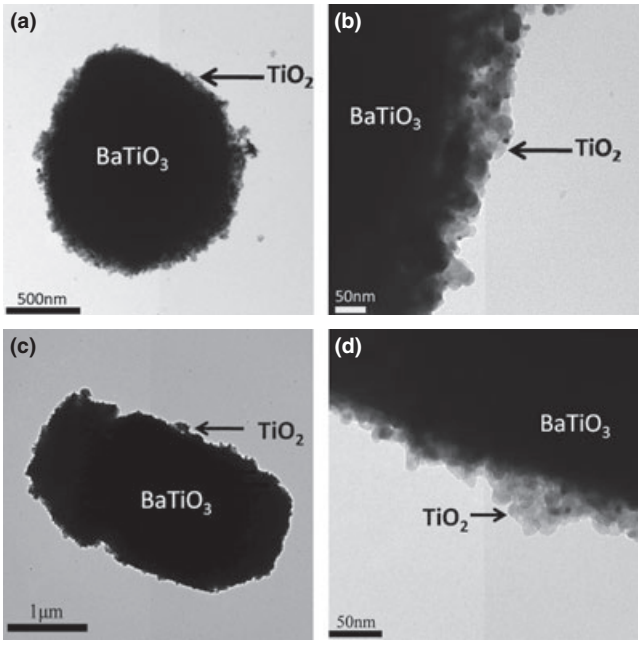

Fig. 2. Bright field TEM images of a platinized heterostructured particle composed of a *mc*-$BaTiO_3$ core and *ns*-TiO_2 shell annealed at (a, b) 600°C and (c, d) 400°C. The entire particles are shown in (a, c) and higher magnification images of the coating are shown in (c, d).

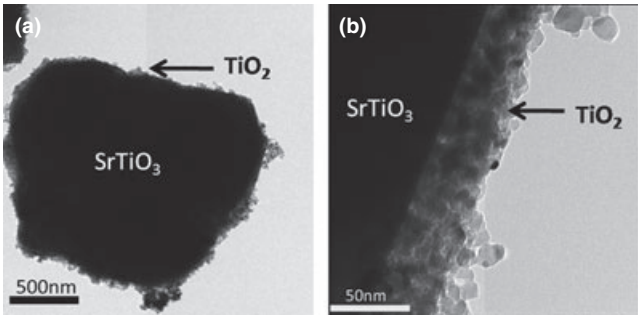

Fig. 3. Bright field TEM images of a platinized heterostructured particle composed of a *mc*-$SrTiO_3$ core and *ns*-TiO_2 shell annealed at 500°C. (a) shows the entire particle and (b) shows a higher magnification of the coating.

phology. The TiO_2 shell completely coats the core with faceted particles that range from 20 to 40 nm in diameter (small black dots on the TiO_2 are attributed to Pt co-catalyst particles). The multiscale core-shell nature of the microstructure is clearly seen to be preserved during high-temperature annealing.

Figures 2 and 3 show BF TEM images of representative particles, respectively, of *mc*-$BaTiO_3$/*ns*-TiO_2 and *mc*-$SrTiO_3$/*ns*-TiO_2. In each case, contrast similar to that described above indicates that the *mc*-core/*ns*-shell heterostructure was achieved for all annealing temperatures and on both core compositions (other heterostructured systems were verified to have such microstructures). Although the overall coverage varies slightly from location to location, the range appears to be 25–100 nm (Figs. 2 and 3), although occasional agglomerates were observed, probably attached through coalescence in solution. This thickness is similar to that of dense TiO_2 films exhibiting domain controlled specific reactivity.[21,29,30] In contrast to dense films, the TiO_2 shells made here have nanoscale grains with nanoscale pores, which should increase the total surface area.

Table I. Summary of the Physical Properties for a Variety of Photocatalysts

Catalyst	T_A (°C)	S (m^2/g)	V_P (cm^3/g)	r_p (Å)	$V_{H2,6\ h}$ (μmol/m^2)	R_{H2} [μmol·(g h)$^{-1}$]
Heterostructures						
mc-BTO/	400	72	0.15	33	9	108
ns-TiO_2	500	61	0.20	48	13	132
	600	44	0.14	43	28	205
c-BTO/	600	36	0.10	43	19	114
ns-TiO_2						
mc-STO/	500	47	0.16	48	22	172
ns-TiO_2	600	41	0.14	55	31	212
c-Al_2O_3/	500	54	0.20	54	13	117
ns-TiO_2	600	35	0.10	32	18	105
Mixtures						
mc-BTO/	RT	28	0.17	152	12	56
P25	500	12	0.25	154	14	28
Components						
P25	RT	49	0.36	154	30	245
P25	500	45	0.42	155	24	180
ns-TiO_2	400	93	0.19	30	11	171
ns-TiO_2	500	70	0.21	43	12	140
ns-TiO_2	600	16	0.06	19	18	48
mc-STO	500	1	0.005	20	3	0.5

The mass specific surface area (S) and pore volumes (V_p), the radius of the most populous pore size (r_P), the total surface area specific volume of hydrogen gas measured after 6 h of photocatalysis ($V_{H2,6\ h}$), and the mass specific molar rate of hydrogen production measured after 6 h (R_{H2}) are reported for a variety of photocatalysts annealed at different temperatures (T_A), where RT is room temperature. For *mc*-$BaTiO_3$ and *mc*-Al_2O_3, no hydrogen was detected. All samples were platinized and were measured using a nominal mass of 0.4 g during experiments.

(2) Surface Area and Pore Characterization

The surface areas (S) and pore morphologies are listed in Table I. S decreases as the annealing temperature (T_A) increases, as expected from thermally driven coarsening. For the *mc*-$BaTiO_3$/*ns*-TiO_2 heterostructured system, S decreases from 72 to 61 to 44 m^2/g (±0.5 m^2/g, which is the error for all S measurements) on increasing T_A from 400°C to 500°C to 600°C, respectively. Similar values were found (see Table I) for the *ns*-TiO_2 shells on all cores, with $S \approx 35$–75 m^2/g. For the *mc*-$BaTiO_3$ and *mc*-$SrTiO_3$ powders, S was ≈1 m^2/g. For the *ns*-TiO_2 powders, S decreased from 93 to 70 to 16 m^2/g on increasing T_A from 400°C to 500°C to 600 °C, respectively. S measured for mixtures of *mc*-$BaTiO_3$ with high surface area powders, such as the P25 mixture, generally were between 20% (high T_A) and 57% (low T_A) of the maximum (low T_A) value for the high surface area powders. S of the heterostructured samples annealed at 400°C and 500°C were slightly lower than those of the freestanding *nc*-TiO_2 annealed at the same temperatures. For the samples annealed at 600°C, the heterostructured samples had larger surface areas. Clearly the nanostructured shell of TiO_2 dramatically improves the overall surface area for the heterostructured systems, compared with mixtures. Also, the microcrystalline core improves the thermal stability of the pores in the *ns*-TiO_2 coating at 600°C. This thermal stability allows for the *ns*-TiO_2 crystallinity and interfacial bonding with the *mc*-cores to improve with only a slight loss in overall surface area.

The pore volume, V_P (cm^3/g), and the radius of the pores with the maximum volumetric contribution, r_P (Å), i.e., r at $dV(r)/dr = 0$, are given in Table I. When $V_P > 0.1$ cm^3/g, the distribution had a defined maximum. When $V_P < 0.1$ cm^3/g, the r_P value had no significant meaning because the distribution is broad and low. Based on the large volumes of pores in the 30–60 nm range, it can be concluded that 2,4-pentanedione acts as a structure-directing agent for TiO_2 shells on microcrystalline powders. The values reported in Table I for P25 are typical for this commercial product,[46] which has a high surface area with large pore volumes. Overall, these

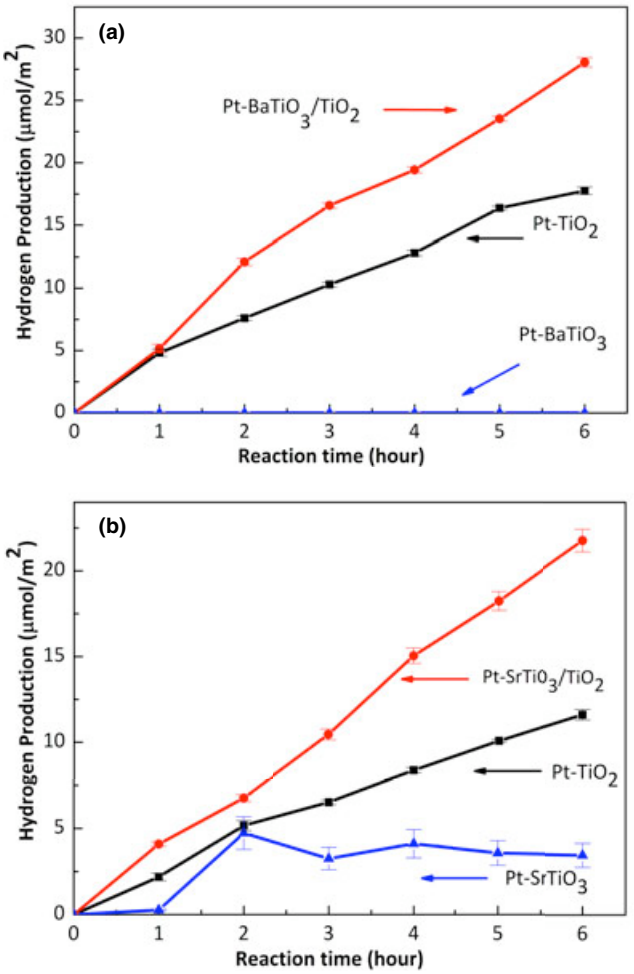

Fig. 4. Time-dependent hydrogen production per surface area from (a) faceted *mc*-BTO/*ns*-TiO_2, *mc*-BTO, and *ns*-TiO_2 annealed at 600°C, and (b) faceted *mc*-STO/*ns*-TiO_2, *mc*-STO, and *ns*-TiO_2 annealed at 500°C. The measurements were taken using platinized (1 wt% Pt) powders suspended in 100 mL 8% methanol-water mixture solution under a UV light.

results indicate that high surface area heterostructured powders were produced with uniform mesoporous shells of thicknesses below 100 nm supported on microcrystalline cores.

(3) Photocatalytic Activity of mc-(Ba,Sr)TiO_3/ns-TiO_2 Powders Annealed at 600°C

Figure 4(a) shows the surface area specific volume of H_2 (V_{H2} in μmol/m^2) produced over time for the *mc*-$BaTiO_3$/*ns*-TiO_2, the *ns*-TiO_2, and the *mc*-$BaTiO_3$ powders. Figure 4(b) shows V_{H2} versus time for the *mc*-$SrTiO_3$/*ns*-TiO_2, *mc*-$SrTiO_3$, and *ns*-TiO_2 powders (all annealed at 600°C). Similar to literature reports,[47] *mc*-$BaTiO_3$ generated no detectable H_2. Although $SrTiO_3$ can split water to produce H_2[48,49] when nanocrystalline, low *S* microcrystalline powders do not generate detectable H_2. The *mc*-$BaTiO_3$/*ns*-TiO_2, *mc*-$SrTiO_3$/*ns*-TiO_2, and *ns*-TiO_2 exhibited linear trends of H_2 production with time (a constant rate). Both *mc*-$BaTiO_3$/*ns*-TiO_2 and *mc*-$SrTiO_3$/*ns*-TiO_2 heterostructured powders clearly exhibit higher activity for H_2 production than either of their components alone, both in overall volume and the average rate (slope), see Table I.

A variety of other types of powders were tested and they are reported in Table I, grouped specifically by the types of photocatalysts, and in Fig. 5, grouped by the annealing temperature. For heterostructured *mc*-$BaTiO_3$/*ns*-TiO_2 treated at 600°C, both faceted and commercial cores yielded similar results, with the *mc*-$BaTiO_3$ being slightly more active. In Table I, values are reported both as $V_{H2,6\ h}$, the area specific volume of hydrogen (μmol/m^2) detected after 6 h of illumination, and as R_{H2}, the time-averaged mass-specific volumetric rate of H_2 produced [$\mu mol\cdot(g\cdot h)^{-1}$]. To simplify comparison, selected results for $V_{H2,6\ h}$ are graphed in Fig. 5. The results indicate that the best photocatalysts are those heterostructured powders with *ns*-TiO_2 shells supported on either *mc*-$BaTiO_3$ or *mc*-$SrTiO_3$ cores annealed at 600°C (no further optimization was carried out).

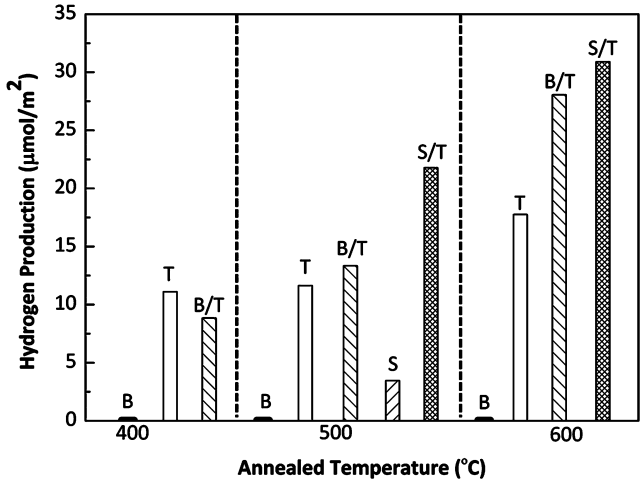

Fig. 5. Total hydrogen production per unit surface area measured after 6 h of a platinized photocatalyst, annealed at different temperatures, was suspended in 100 mL of an 8% methanol-water solution and exposed to UV illumination. The abbreviations of the photocatalyst are B: *mc*-$BaTiO_3$, T: *ns*-TiO_2, B/T: *mc*-$BaTiO_3$/*ns*-TiO_2, S: *mc*-$SrTiO_3$, S/T: *mc*-$SrTiO_3$/*ns*-TiO_2.

(4) Dependence of Photocatalytic Activity on Annealing Temperature

The measured photocatalytic activity depends on the annealing temperature. The H_2 production rates decreased (both $V_{H2,6\ h}$ and R_{H2}) for P25 when annealed at 500°C (compared with as-received), concomitant with a decrease in *S*. In contrast, the H_2 production rates increased (both $V_{H2,6\ h}$ and R_{H2}) with annealing temperature for heterostructured powders, even though *S* decreased. This increased activity can be ascribed to improved crystallinity of the *ns*-TiO_2 coating or improved bonding between the *ns*-TiO_2 coating and the *mc*-(Ba,Sr)TiO_3 core. For our freestanding *ns*-TiO_2, H_2 production per unit area ($V_{H2,6\ h}$) increased with annealing temperature significantly (from 11 to 18 μmol/m^2), but not as significantly as for the heterostructures, although the H_2 production per unit mass (R_{H2}) decreased by a larger percentage [from 171 to 48 $\mu mol\cdot(g\cdot h)^{-1}$].

The increase in $V_{H2,6h}$ on annealing *ns*-TiO_2 (which is opposite to the behavior of P25) is likely related to improved crystallinity with annealing. The overall decrease in R_{H2} illustrates that the decrease in *S* is more important than the per unit surface area improvement related to increased crystallinity in *ns*-TiO_2. As the increase (with annealing temperature) in $V_{H2,6\ h}$ on annealing the heterostructures is greater than the marginal increase for the *ns*-TiO_2, it is unlikely to be caused by a simple increase in crystallinity. Moreover, as R_{H2} increased with annealing for the heterostructures, the improved activity of the heterostructures is more likely the result of improved structural characteristics at the interface of the *mc*-(Ba,Sr)TiO_3 cores and the *ns*-TiO_2 shells, allowing photogenerated carriers in the cores to be transferred to the high surface area shells. This would be similar to the activity improvements of dense TiO_2 coatings on $BaTiO_3$.[21,29,30]

(5) Photocatalytic Activity of Control Heterostructures and Mixtures

Experiments were conducted using *mc*-Al_2O_3/*ns*-TiO_2 heterostructured catalysts processed under the same conditions as the *mc*-$BaTiO_3$/*ns*-TiO_2 powders. At T_A = 500°C, a similar photocatalytic activity was observed for freestanding *ns*-TiO_2 or *ns*-TiO_2 supported on either light absorbing [(Ba,Sr)TiO_3] or nonabsorbing (Al_2O_3) cores. At T_A = 600°C, on the other hand, R_{H2} increases dramatically for the heterostructured photocatalysts having light absorbing (Ba,Sr)TiO_3 cores and decreases for the nonabsorbing Al_2O_3 cores and free-standing particles ($V_{H2,6\ h}$ increases for all owing to improved crystallinity in the *ns*-shells). These findings indicate that the *mc*-core plays a significant role in the performance of the heterostructured photocatalysts when the annealing temperature is high, likely owing to the improved interface between the shell and core.

Experiments were carried out using sonomechanical mixtures of *mc*-$BaTiO_3$ and P25. In contrast to the *ns*-TiO_2 powders annealed at 500°C and 600°C, *mc*-$BaTiO_3$ mixed with P25 shows significantly lower H_2 production than P25 alone, and much less than the heterostructures. For the mixtures, increased annealing temperatures do not affect $V_{H2,6\ h,}$ but significantly decrease R_{H2}, in contrast to the behavior of the heterostructures. The decreased R_{H2} value in the mixture is likely related to the loss in total surface area, which also indicates that improved interphase bonding does not improve the performance of the mixture significantly. This is understandable because only some of the (Ba,Sr)TiO_3 interfaces will be in contact with P25 and the thickness of the P25 at any given interface remains unknown, as is the integrity of the interfaces. In the heterostructures, each (Ba,Sr)TiO_3 particle is coated with ≈50 (±25) nm of active TiO_2 and annealing leads to a decrease in surface area, as expected, but an increase in the R_{H2} values. These control experiments suggest that the light absorbing microcrystalline core plays an important role in the activity of the heterostructured photocatalysts.

(6) Discussion of $BaTiO_3$ and $SrTiO_3$ as Cores

The most important observation made above is that heterostructured powders, consisting of microcrystalline (Ba,Sr)TiO_3 cores with nanostructured nanoporous TiO_2 shells, are more active than either the microcrystalline cores or nanostructured shells alone. This implies that the properties of photocatalysts can be improved if the material has multiple length scales. In addition, when the core did not absorb light, no improvement in the properties was observed. This indicates that carriers photogenerated in the core participate in the reactions on the shell. These arguments are also consistent with observations made on dense titania films supported on $BaTiO_3$ substrates.[29,30] As such, transfer across the interface should be critical. The observed improvement of the photocatalytic hydrogen production from heterostructured powders annealed at 600°C can be understood as arising from improved transfer of carriers across the interface. We will discuss this model below.

The absorption coefficients for anatase and rutile are 2×10^3 and 1×10^5/cm, respectively[30,50]; $BaTiO_3$ has a similar value to that of rutile.[30] Ignoring interfacial scattering, a 50 (100) nm thick anatase layer will absorb only ≈1 (≈2)% of incident photons, while similar rutile ($BaTiO_3$) layers will absorb ≈40 (≈67)% of the photons. As our TiO_2 coatings are ≈90% anatase, the majority of photons will be absorbed in the first few hundred nanometers of the $BaTiO_3$ microcrystal. The observation that the *mc*-Al_2O_3/*ns*-TiO_2 coatings exhibit similar photocatalytic activity to *ns*-TiO_2 alone further supports the argument that carriers photogenerated in the core contribute the activity of *mc*-$BaTiO_3$/*ns*-TiO_2 catalysts.

Carriers photogenerated in the core must past through the interface to participate in shell reactions. Interfacial transfer will increase, generally, with improved interfacial bonding, which improves, generally, with annealing. The photocatalytic activity per unit surface area ($V_{H2,6\ h}$) and per unit mass (R_{H2}) increased with T_A for the heterostructured powders. For *ns*-TiO_2 or *mc*-Al_2O_3/*ns*-TiO_2, $V_{H2,6\ h}$ increased slightly with T_A whereas R_{H2} decreased substantially with increased T_A. The latter observations are attributed to increased crystallinity of our *ns*-TiO_2 powders with annealing, while the differences observed for the heterostructures with light absorbing cores is attributable to improved contact at the heterostructured interface, leading to enhanced photocatalytic activity per unit mass with increasing annealing temperature, despite the loss of overall surface area. Further support is provided by the lack of improvement in H_2 production for sonomechanical mixtures of $BaTiO_3$ and P25, which have poorly defined interfacial characteristics between the two phases.

Simplified band structure diagrams for ideal heterostructures are given in Fig. 6. The conduction band positions[51–54] and the bandgap energies[55–58] of $BaTiO_3$ and TiO_2 were assumed to be the same, although the real difference between them is ≈0.2 V. A work function of 4.2 eV (that of TiO_2[59]) was used to situate the Fermi level relative to the vacuum level; we assumed the Fermi level was ≈0.1 eV[60,61] below the conduction band edge of the n-type semiconductors. The effects of interface states were ignored, the redox potential difference between H_2/H^+ and O_2/O^- was set at 1.23 V,[7]

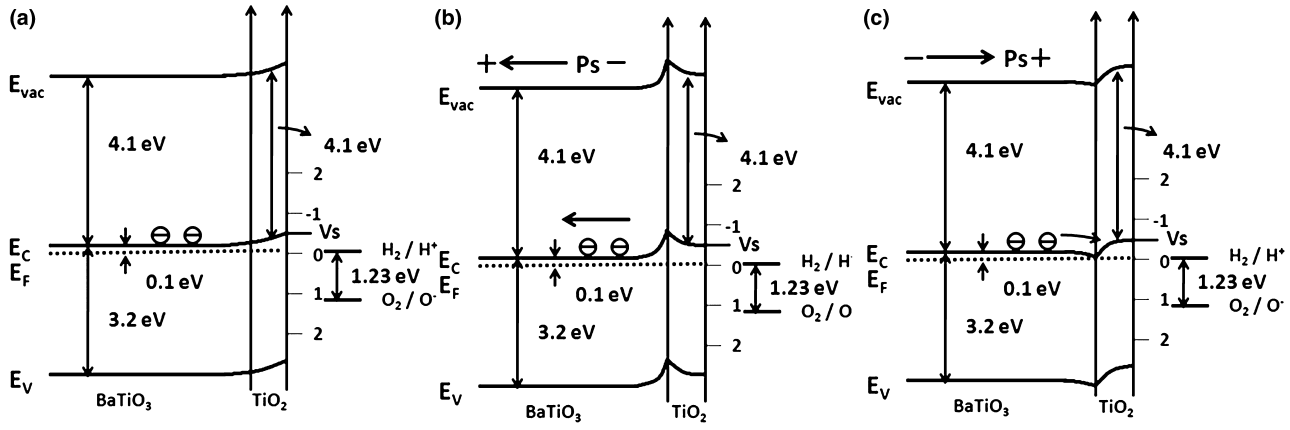

Fig. 6. A highly simplified schematic band structure diagram of heterostructured $BaTiO_3/TiO_2$ with (a) no, (b) negative, and (c) positive polarization (E_{vac}, E_c, E_f, and E_v represent the energy for the vacuum level, the conduction band, the Fermi level, and the valance band, respectively. P_s refers to spontaneous polarization. The hydrogen and oxygen redox level are shown in the right).

and we represent electrochemical equilibrium between the solid and solution by matching the Fermi level with the solution H_2/H^+ level. The TiO_2 surface potential was set to a value determined from flat band measurements assuming the interface states with the solution are unperturbed by the heterostructure.[7]

Figure 6(a) describes the situation where there is no trapped interfacial charge or polarization at the $BaTiO_3/TiO_2$ interface. As the coating thickness is smaller than the depletion layer width, the depletion layer extends into the $BaTiO_3$.[19] In general, the thickness of the depletion layer should be about 100 nm in titanates (assuming a typical doping level).[19] Figures 6(b) and (c) show schematics in which surfaces are charged, respectively, negative and positive, by a ferroelectric polarization. These interfacial charges could also represent local chemical variations at the interfaces, although the ferroelectric charge is expected to be significantly larger than that from local chemical variations. For example, the lower electron affinity and higher isoelectric point of $SrTiO_3$ compared with TiO_2 can result in a potential step at the interface between them.[62] The bands are bent upward at the interface with the negative polarization (charge) and downward with the positive. The bands in the TiO_2 cannot relax to the bulk value in these cases because they are too thin to accommodate the two surface charges.

The reactivity of such a particle will depend on the photon absorption location, carrier diffusion length, and carrier interfacial transfer. In the case of anatase-coated $(Ba,Sr)TiO_3$ having no trapped interfacial charge, much of the light is absorbed in the *mc*-bulk where there is no electric field to separate carriers. Ferroelectric polarization (surface charge) acts to increase the width of band bending and the likeliness a photon is absorbed in a region with an electric field. With positive (negative) polarization/charge, electrons (holes) in $BaTiO_3$ move toward the interface and can be injected into the TiO_2 if they have enough energy to overcome the barrier[63] or if they tunnel through it[29,30] (holes do not have a barrier). It has been shown elsewhere that surfaces of domains with positive polarization promote reduction in both bare $BaTiO_3$ and in TiO_2 coated $BaTiO_3$.[29,30] Overall, heterostructured *mc*-$BaTiO_3$/*ns*-TiO_2 should display enhanced photocatalytic activity compared with the separate phases if these diagrams represent the different extremes of interfaces. However, if interfacial transfer is significantly impeded or no light absorption occurs in the core, then the heterostructures will have similar or worse properties than the coatings themselves. All of the above-described observations agree with this model.

Heterostructured catalysts with $SrTiO_3$ cores have reactivities similar to those with ferroelectric $BaTiO_3$ cores. For $(Ba,Sr)TiO_3$ powders and ceramics, similar maximum values of reactivity were found for three compositions: $BaTiO_3$, $Ba_{0.74}Sr_{0.26}TiO_3$, and $SrTiO_3$.[31,32] Major factors that were suggested to influence the reactivity of the $(Ba,Sr)TiO_3$ cores were the remanent polarization, the space charge width variations with the dielectric constant, the band edge position, and the absorption cross-section for UV light.[31,32] Our results correlate well to the observations for microcrystalline $(Ba,Sr)TiO_3$ powders in terms of the relative reactivity of the $BaTiO_3$ and $SrTiO_3$ cores. We take this as further evidence that the ideal heterostructured *mc*-$BaTiO_3$/*ns*-TiO_2 catalysts absorb light in the core and shuttle carriers to the high surface area shells. Enhanced photocatalytic activity of heterostructured $SrTiO_3/TiO_2$ nanocomposites, such as nanofiber and nanotube, has previously been reported.[62,64–67] The enhancement was attributed to electron transfer from $SrTiO_3$ to TiO_2, owing to the interfacial dipole described above.[64] No matter their origin, interfacial charges cause band bending in the core where absorption is occurring. This affords an internal field in the core, allowing charges to be separated, shuttled to the TiO_2 shells (as long as interfacial transfer is possible), and reacted with solution species, and used in H_2 production. Separation of the absorption and reaction locations in heterostructured photocatalysts offers a new approach to design ceramic photocatalysts.

IV. Conclusions

The *mc*-$(Ba,Sr)TiO_3$ core/*ns*-TiO_2 shell heterostructured ceramics exhibit enhanced photocatalytic activity for hydrogen production, when compared with any of their components alone or mixtures thereof. The improved reactivity of the heterostructure is attributed to the combined efficient absorption and charge separation in the *mc*-core, efficient transfer across the *mc*-core/*ns*-shell interface, and high surface area and reactivity of the *ns*-TiO_2 shell. These attributions were supported by comparing the reactivity of the heterostructures to the reactivities of freestanding *ns*-TiO_2, heterostructures with nonlight-absorbing cores, and mechanical mixtures of *mc*-cores with P25.

Acknowledgment

This study was supported by National Science Foundation (DMR 0804770) and the PA DCED.

References

[1]A. Fujishima and K. Honda, "Electrochemical Photolysis of Water at a Semiconductor Electrode," *Nature*, **238**, 37–8 (1972).
[2]A. Nozik, "Photoelectrochemistry: Applications to Solar Energy Conversion," *Annu. Rev. Phys. Chem.*, **29**, 189–222 (1978).
[3]A. J. Bard, "Design of Semiconductor Photoelectrochemical Systems for Solar Energy Conversion," *J. Phys. Chem.*, **86**, 172 (1982).
[4]S. Licht, "Multiple Bandgap Semiconductor/Electrolyte Solar Energy Conversion," *J. Phys. Chem. B*, **105**, 6281–94 (2001).
[5]F. E. Osterloh, "Inorganic Materials as Catalysts for Photochemical Splitting of Water," *Chem. Mater.*, **20** [1] 35–54 (2008).
[6]A. Kudo and Y. Miseki, "Heterogeneous Photocatalyst Materials for Water Splitting," *Chem. Soc. Rev.*, **38**, 253–78 (2009).
[7]S. R. Morrison, *Electrochemistry at Semiconductor and Oxidized Metal Electrodes*. pp. 401. Plenum Press, New York, 1980.
[8]K. Maeda and K. Domen, "Photocatalytic Water Splitting: Recent Progress and Future Challenges," *J. Phys. Chem. Lett.*, **1** [18] 2655–61 (2010).
[9]R. Vogel, K. Pohl, and H. Weller, "Sensitization of Highly Porous, Polycrystalline TiO_2 Electrodes by Quantum Sized CdS," *Chem. Phys. Lett.*, **174** [3–4] 241–6 (1990).
[10]S. Hotchandani and P. V. Kamat, "Charge-Transfer Processes in Coupled Semiconductor Systems. Photochemistry and Photoelectrochemistry of the Colloidal Cadmium Sulfide-Zinc Oxide System," *J. Phys. Chem.*, **96** [16] 6834–9 (1992).
[11]R. Vogel, P. Hoyer, and J. Weller, "Quantum-Sized PbS, CdS, Ag_2S, Sb_2S_3, and Bi_2S_3 Particles as Sensitizers for Various Nanoporous Wide-Bandgap Semiconductors," *J. Phys. Chem.*, **98**, 3183–8 (1994).
[12]S. H. Elder, F. M. Cot, Y. Su, S. M. Heald, A. M. Tyryshkin, M. K. Bowman, Y. Gao, A. G. Joly, M. L. Balmer, A. C. Kolwaite, K. A. Magrini, and D. M. Blake, "The Discovery and Study of Nanocrystalline TiO_2-(MoO_3) Core-Shell Materials," *J. Am. Chem. Soc.*, **122** [21] 5138–46 (2000).
[13]T. Hirakawa and P. V. Kamat, "Charge Separation and Catalytic Activity of Ag@TiO_2 Core-Shell Composite Clusters Under UV-Irradiation," *J. Am. Chem. Soc.*, **127** [11] 3928–34 (2005).
[14]J. H. Luo and P. A. Maggard, "Hydrothermal Synthesis and Photocatalytic Activities of $SrTiO_3$-Coated Fe_2O_3 and $BiFeO_3$," *Adv. Mater.*, **18** [4] 514–7 (2006).
[15]K. Maeda, K. Teramura, D. Lu, N. Saito, Y. Inoue, and K. Domen, "Noble-Metal/Cr_2O_3 Core/Shell Nanoparticles as a Cocatalyst for Photocatalytic Overall Water Splitting," *Angew. Chem. Int. Ed.*, **45** [46] 7806–9 (2006).
[16]B. Gao, Y. J. Kim, A. K. Chakraborty, and W. I. Lee, "Efficient Decomposition of Organic Compounds with $FeTiO_3/TiO_2$ Heterojunction Under Visible Light Irradiation," *Appl. Catal. B*, **83** [3–4] 202–7 (2008).
[17]S. Li, Y. H. Lin, B. P. Zhang, J. F. Li, and C. W. Nan, "$BiFeO_3/TiO_2$ Core-Shell Structured Nanocomposites as Visible-Active Photocatalysts and Their Optical Response Mechanism," *J. Appl. Phys.*, **105** [5] 054310 (2009).
[18]K. Domen, "Characterization of Photoexcitation Processes on Solid Surfaces," pp. 1. in *Surface Photochemistry*, Edited by M. Anpo. J. Wiley & Sons, Chichester, 1996.
[19]W. J. Albery and N. B. Philip, "The Transport and Kinetics of Photogenerated Carriers in Colloidal Semiconductor Electrode Particles," *J. Electrochem. Soc.*, **131** [2] 315–25 (1984).
[20]A. Nozik, "Photochemical Diodes," *Appl. Phys. Lett.*, **30**, 567–9 (1977).

[21]N. V. Burbure, P. A. Salvador, and G. S. Rohrer, "Influence of Dipolar Fields on the Photochemical Reactivity of Thin Titania Films on $BaTiO_3$ Substrates," *J. Am. Ceram. Soc.*, **89** [9] 2943–5 (2006).

[22]J. L. Giocondi and G. S. Rohrer, "Structure Sensitivity of Photochemical Oxidation and Reduction Reactions on $SrTiO_3$ Surfaces," *J. Am. Ceram. Soc.*, **86** [7] 1182–9 (2003).

[23]Y. Inoue, K. Sato, K. Sato, and H. Miyama, "Photoassisted Water Decomposition by Ferroelectric Lead Zirconate Titanate Ceramics with Anomalous Photovoltaic Effects," *J. Phys. Chem.*, **90**, 2809–10 (1986).

[24]Y. Inoue, K. Sato, and K. Sato, "Photovoltaic and Photocatalytic Behavior of a Ferroelectric Semiconductor, Lead Strontium Zirconate Titanate, with a Polarization Axis Perpendicular to the Surface," *J. Chem. Soc. Farad. Trans.*, **85**, 1765–74 (1989).

[25]J. L. Giocondi and G. S. Rohrer, "Spatially Selective Photochemical Reduction of Silver on the Surface of Ferroelectric Barium Titanate," *Chem. Mater.*, **13**, 241–2 (2001).

[26]J. L. Giocondi and G. S. Rohrer, "Spatial Separation of Photochemical Oxidation and Reduction Reactions on the Surface of Ferroelectric Barium Titanate," *J. Phys. Chem. B*, **105**, 8275–7 (2001).

[27]S. Dunn, P. M. Jones, and D. E. Gallardo, "Photochemical Growth of Silver Nanoparticles on c(−) and c(+) Domains on Lead Zirconate Titanate Thin Films," *J. Am. Ceram. Soc.*, **129** [28] 8724–8 (2007).

[28]J. L. Giocondi and G. S. Rohrer, "The Influence of the Dipolar Field Effect on the Photochemical Reactivity of $Sr_2Nb_2O_7$ and $BaTiO_3$ Microcrystals," *Top. Catal.*, **49** [1–2] 18–23 (2008).

[29]N. V. Burbure, P. A. Salvador, and G. S. Rohrer, "Photochemical Reactivity of Titania Films on $BaTiO_3$ Substrates: Influence of Titania Phase and Orientation," *Chem. Mater.*, **22**, 5831–7 (2010).

[30]N. V. Burbure, P. A. Salvador, and G. S. Rohrer, "Photochemical Reactivity of Titania Films on $BaTiO_3$ Substrates: Origin of Spatial Selectivity," *Chem. Mater.*, **22**, 5823–30 (2010).

[31]A. Bhardwaj, N. V. Burbure, and G. S. Rohrer, "Enhanced Photochemical Reactivity at the Ferroelectric Phase Transition in $Ba_{1-x}Sr_xTiO_3$," *J. Am. Ceram. Soc.*, **93**, 4129–34 (2010).

[32]A. Bhardwaj, N. V. Burbure, A. Gamalski, and G. S. Rohrer, "Composition Dependence of the Photochemical Reduction of Ag by $Ba_{1-x}Sr_xTiO_3$," *Chem. Mater.*, **22**, 3527–34 (2010).

[33]D. Tiwari and S. Dunn, "Photochemistry on a Polarisable Semiconductor: What Do We Understand Today?" *J. Mater. Sci.*, **44**, 5063–79 (2009).

[34]A. Fujishima, T. N. Rao, and D. A. Tryk, "Titanium Dioxide Photocatalysis," *J. Photochem. Photobiol. C*, **1** [1] 1–21 (2000).

[35]R. Asahi, T. Morikawa, T. Ohwaki, K. Aoki, and Y. Taga, "Visible-Light Photocatalysis in Nitrogen-Doped Titanium Oxides," *Science*, **293** [5528] 269–71 (2001).

[36]J. S. Jang, W. Li, S. H. Oh, and J. S. Lee, "Fabrication of CdS/TiO_2 Nano-Bulk Composite Photocatalysts for Hydrogen Production from Aqueous H_2S Solution Under Visible Light," *Chem. Phys. Lett.*, **425** [4–6] 278–82 (2006).

[37]J. S. Jang, S. M. Ji, S. W. Bae, H. C. Son, and J. S. Lee, "Optimization of CdS/TiO_2 Nano-Bulk Composite Photocatalysts for Hydrogen Production from Na_2S/Na_2SO_3 Aqueous Electrolyte Solution Under Visible Light ($\lambda \geq 420$ nm)," *J. Photochem. Photobiol. A Chem.*, **188** [1] 112–9 (2007).

[38]M. Ye, Q. Zhang, Y. Hu, J. Ge, Z. Lu, L. He, Z. Chen, and Y. Yin, "Magnetically Recoverable Core–Shell Nanocomposites with Enhanced Photocatalytic Activity," *Chem. Eur. J.*, **16** [21] 6243–50 (2010).

[39]A. V. Vorontsov, I. V. Stoyanova, D. V. Kozlov, V. I. Simagina, and E. N. Savinov, "Kinetics of the Photocatalytic Oxidation of Gaseous Acetone Over Platinized Titanium Dioxide," *J. Catal.*, **189** [2] 360–9 (2000).

[40]Z. Q. He, L. Xie, J. J. Tu, S. Song, W. P. Liu, Z. W. Liu, J. Q. Fan, Q. Liu, and J. M. Chen, "Visible Light-Induced Degradation of Phenol Over Iodine-Doped Titanium Dioxide Modified with Platinum: Role of Platinum and the Reaction Mechanism," *J. Phys. Chem. C*, **114** [1] 526–32 (2010).

[41]V. P. Jain and A. Proctor, "Photocatalytic Production and Processing of Conjugated Linoleic Acid-Rich Soy Oil," *J. Agric. Food Chem.*, **54** [15] 5590–6 (2006).

[42]H. Kato and A. Kudo, "Visible-Light-Response and Photocatalytic Activities of TiO_2 and $SrTiO_3$ Photocatalysts Codoped with Antimony and Chromium," *J. Phys. Chem. B*, **106** [19] 5029–34 (2002).

[43]J. Y. Shi, J. Chen, Z. C. Feng, T. Chen, Y. X. Lian, X. L. Wang, and C. Li, "Photoluminescence Characteristics of TiO_2 and Their Relationship to the Photoassisted Reaction of Water/Methanol Mixture," *J. Phys. Chem. C*, **111** [2] 693–9 (2007).

[44]A. Sclafani and J. M. Herrmann, "Comparison of the Photoelectronic and Photocatalytic Activities of Various Anatase and Rutile Forms of Titania in Pure Liquid Organic Phases and in Aqueous Solutions," *J. Phys. Chem.*, **100** [32] 13655–61 (1996).

[45]D. C. Hurum, A. G. Agrios, K. A. Gray, T. Rajh, and M. C. Thurnauer, "Explaining the Enhanced Photocatalytic Activity of Degussa P25 Mixed-Phase TiO_2 Using EPR," *J. Phys. Chem. B*, **107** [19] 4545–9 (2003).

[46]T. Ohno, K. Sarukawa, K. Tokieda, and M. Matsumura, "Morphology of a TiO_2 Photocatalyst (Degussa, P-25) Consisting of Anatase and Rutile Crystalline Phases," *J. Catal.*, **203** [1] 82–6 (2001).

[47]Y. Yamashita, M. Tada, M. Kakihana, M. Osada, and K. Yoshida, "Synthesis of RuO_2-Loaded $BaTi_nO_{2n+1}$ (n = 1, 2 and 5) Using a Polymerizable Complex Method and its Photocatalytic Activity for the Decomposition of Water," *J. Mater. Chem.*, **12** [6] 1782–6 (2002).

[48]K. Yamaguti and S. Sato, "Photolysis of Water Over Metallized Powdered Titanium-Dioxide," *J. Chem. Soc. Farad. Trans.*, **81**, 1237–46 (1985).

[49]T. Ishii, H. Kato, and A. Kudo, "H_2 Evolution from an Aqueous Methanol Solution on $SrTiO_3$ Photocatalysts Co-Doped with Chromium and Tantalum Ions Under Visible Light Irradiation," *J. Photochem. Photobiol. A Chem.*, **163** [1–2] 181–6 (2004).

[50]Y. R. Park and K. J. Kim, "Structural and Optical Properties of Rutile and Anatase TiO_2 Thin Films: Effects of Co Doping," *Thin Solid Films*, **484** [1–2] 34–8 (2005).

[51]H. H. Kung, H. S. Jarrett, A. W. Sleight, and A. Ferretti, "Semiconducting Oxide Anodes in Photoassisted Electrolysis of Water," *J. Appl. Phys.*, **48** [6] 2463–9 (1977).

[52]L. Kavan, M. Grätzel, S. E. Gilbert, C. Klemenz, and H. J. Scheel, "Electrochemical and Photoelectrochemical Investigation of Single-Crystal Anatase," *J. Am. Chem. Soc.*, **118** [28] 6716–23 (1996).

[53]K. Sayama and H. Arakawa, "Photocatalytic Decomposition of Water and Photocatalytic Reduction of Carbon Dioxide Over Zirconia Catalyst," *J. Phys. Chem.*, **97** [3] 531–3 (1993).

[54]S. Sakthivel and H. Kisch, "Daylight Photocatalysis by Carbon-Modified Titanium Dioxide," *Angew. Chem. Int. Ed.*, **42** [40] 4908–11 (2003).

[55]F. A. Grant, "Properties of Rutile (Titanium Dioxide)," *Rev. Mod. Phys.*, **31** [3] 646–74 (1959).

[56]R. C. Casella and S. P. Keller, "Polarized Light Transmission of $BaTiO_3$ Single Crystals," *Phys. Rev.*, **116** [6] 1469 (1959).

[57]M. Cardona, "Optical Properties and Band Structure of $SrTiO_3$ and $BaTiO_3$," *Phys. Rev.*, **140** [2A] A651 (1965).

[58]J. Pascual, J. Camassel, and H. Mathieu, "Fine Structure in the Intrinsic Absorption Edge of TiO_2," *Phys. Rev. B*, **18** [10] 5606 (1978).

[59]A. Imanishi, E. Tsuji, and Y. Nakato, "Dependence of the Work Function of TiO_2 (Rutile) on Crystal Faces, Studied by a Scanning Auger Microprobe," *J. Phys. Chem. C*, **111** [5] 2128–32 (2007).

[60]R. G. Breckenridge and W. R. Hosler, "Electrical Properties of Titanium Dioxide Semiconductors," *Phys. Rev.*, **91** [4] 793 (1953).

[61]C. N. Berglund and H. J. Braun, "Optical Absorption in Single-Domain Ferroelectric Barium Titanate," *Phys. Rev.*, **164** [2] 790 (1967).

[62]Y. Diamant, S. G. Chen, O. Melamed, and A. Zaban, "Core-Shell Nanoporous Electrode for Dye Sensitized Solar Cells: The Effect of the $SrTiO_3$ Shell on the Electronic Properties of the TiO_2 Core," *J. Phys. Chem. B*, **107** [9] 1977–81 (2003).

[63]X. Zhang, L. Zhang, T. Xie, and D. Wang, "Low-Temperature Synthesis and High Visible-Light-Induced Photocatalytic Activity of $BiOI/TiO_2$ Heterostructures," *J. Phys. Chem. C*, **113** [17] 7371–8 (2009).

[64]T. P. Cao, Y. J. Li, C. H. Wang, C. L. Shao, and Y. C. Liu, "A Facile In Situ Hydrothermal Method to $SrTiO_3/TiO_2$ Nanofiber Heterostructures with High Photocatalytic Activity," *Langmuir*, **27** [6] 2946–52 (2011).

[65]X. M. Zhang, K. F. Huo, L. S. Hu, Z. W. Wu, and P. K. Chu, "Synthesis and Photocatalytic Activity of Highly Ordered TiO_2 and $SrTiO_3/TiO_2$ Nanotube Arrays on Ti Substrates," *J. Am. Ceram. Soc.*, **93** [9] 2771–8 (2010).

[66]J. Yan, Y. Zhu, Y. Tang, and S. Zheng, "Nitrogen-Doped $SrTiO_3/TiO_2$ Composite Photocatalysts for Hydrogen Production Under Visible Light Irradiation," *J. Alloys Compd.*, **472** [1–2] 429–33 (2009).

[67]J. Zhang, J. H. Bang, C. C. Tang, and P. V. Kamat, "Tailored TiO_2-$SrTiO_3$ Heterostructure Nanotube Arrays for Improved Photoelectrochemical Performance," *ACS Nano*, **4** [1] 387–95 (2010). □